

Compression of hollow microspheres by laser radiation

N. G. Basov, Yu. A. Zakharenkov, N. N. Zorev, A. A. Kologrivov,
O. N. Krokhin, A. A. Rupasov, G. V. Sklizkov, and A. S. Shikanov

P. N. Lebedev Physics Institute USSR Academy of Sciences
(Submitted May 17, 1976)
Zh. Eksp. Teor. Fiz. 71, 1788-1798 (November 1976)

Results are presented of an investigation of the interaction between the radiation from the "Calmar" nine-channel laser assembly and hollow microspheres. The fraction of light energy absorbed by the plasma is determined by various methods. The effect of initial perturbations on the stability of compression of a hollow target is elucidated. A volume compression by a factor ~ 200 is recorded for a homogeneous glass microsphere.

PACS numbers: 52.50Jm 42.60 Nj

1. INTRODUCTION

The experiments performed to date on solid and hollow-shell targets have yielded evidence of the existence of strong compression of the material in the center of the target.^[1-7] The final compressions and the temperature, as is well known,^[8-11] are determined by the mechanism whereby the high-power laser-radiation energy is absorbed and transformed into the plasma energy, by the dynamic instability of the compression, and by processes that take place in the plasma corona. We describe in this paper the results of an experimental investigation of the interaction of laser radiation of nanosecond duration with hollow microscopic spheres. Various methods were used to determine the fraction of the energy absorbed by the plasma and the spectral composition and the energy of the radiation scattered by the plasma. We investigated the influence of the initial perturbations on the stability of the compression of the microsphere. With the aid of pinpoint cameras we reg-

istered a 200-fold volume compression of a shell with a homogeneous wall.

2. EXPERIMENTAL SETUP

A. The Calmar laser setup and the focusing system

A diagram of the laser setup and of the diagnostic apparatus is shown in Fig. 1. In contrast to preceding experiments,^[12] the active element of the master laser 1 of the nine-channel neodymium-laser installation was an yttrium-aluminum garnet. As a result, the emission-line half-width at the exit from the laser installation was $\Delta\lambda \sim 10 \text{ \AA}$ ($\lambda_0 = 10640 \text{ \AA}$, Fig. 2). When the yttrium-aluminum garnet was used, we employed an additional amplifier 2 to raise the energy of the light beam in front of the shaping Kerr shutter 3 to $\sim 0.1-0.2 \text{ J}$. From the Kerr shutter, which was controlled by a laser-fired discharge gap 4, the shortened light pulse was fed to a system of preamplification stages 5. We note that to increase the radiation contrast the light beam passed twice through the Kerr shutter. This pulse-shaping system is equivalent to a system with two shutters placed in tandem and ideally synchronized. The radiation passed twice through the first two preamplifiers, while in the last three stages the amplification was with the beam diverging. Next, a beam splitting system 11 and final amplifiers formed the nine laser beams, which were focused from different directions onto a spherical target placed at the center of a vacuum chamber. To increase the contrast, several "passive" shutters 6 with low ($< 10\%$) initial transmission were placed in the system.

The laser energy in the described series of experiments reached 150 J at a light-pulse duration at the

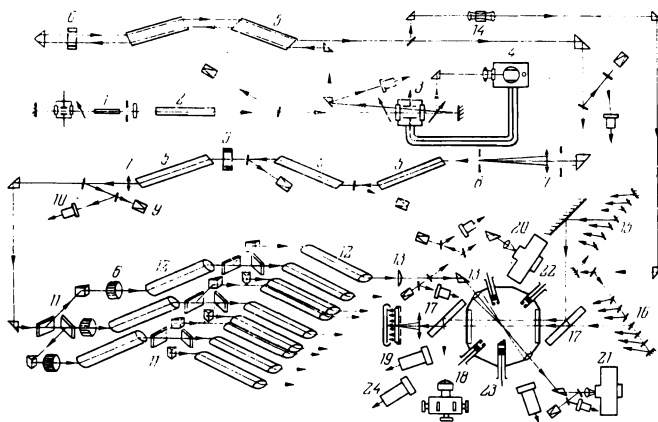


FIG. 1. Experimental setup: 1—driving laser, 2—preamplifier, 3—Kerr shutter, 4—laser-fired discharge gap, 5—double pass amplifiers, 6—saturable filters, 7—lens, 8—diaphragm, 9—calorimeters, 10—coaxial photocells, 11—beam-splitting systems, 12—power-amplification stages, 13—optical components of the system for focusing on the target, 14—KDP crystal, 15—optical delay for multiframe interferometry, 16—optical delay for multiframe Schlieren photography, 17—Jamin interferometer, 18—multiframe interference photographic camera, 19—multiframe Schlieren systems, 20, 21—spectrographs, 22—x-ray pinpoint cameras, 23—multi-channel x-ray film detector, 24—neutron detectors.

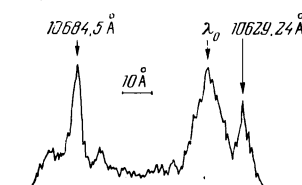


FIG. 2. Spectrum of the radiation incident on the target, $\lambda_0 = 10640 \text{ \AA}$. The references were third-order the mercury lines Hg 3561.5 Å and Hg 3543.08 Å the first-order positions corresponded to the wavelengths 10684.5 Å and 10629.24 Å.

base $\tau \approx 2.5$ nsec and at a rise time $\tau_r \approx 0.5$ nsec. The use of a somewhat lower laser energy than in the preceding experiments was dictated mainly by the lower gain of the neodymium glass for the narrow emission line, and also by the stringent requirements on the radiation contrast (i. e., on the ratio of the energy of the heating pulse to the energy of the "parasitic" radiation preceding the heating pulse and capable of damaging the target). Since the energy needed to evaporate the employed hollow microsphere was $\lesssim 10^{-3}$ J, the required contrast was $\sim 10^6$. The control experiments performed with the laser-fired discharge gap turned off (in which case there was no heating pulse and all that reached the target was the background generation, consisting of the amplified radiation of the pump lamps, the superradiance, and the laser radiation passing through the shutter) have revealed no noticeable traces of damage in the hollow-shell target even after several "idle" laser flashes.

The radiation laser from the amplifier stages was focused with the aid of nine two-lens (13) systems (with effective focal length $F = 20$ cm) on the target. The degree of linear polarization of each beam on the surface of the target was low, a fact due, in particular, to the depolarization by the prisms of the guidance system. The optical paths of each beam were equalized both in the beam-splitting systems 11 and in the system that guided the radiation to the target. As a result, the difference between the optical paths of the "fastest" and "slowest" beams was less than 2 cm, i. e., the delay time was less than 10^{-10} sec.

Owing to the Fresnel losses in the guidance system and in the diagnostic-apparatus elements, the optical energy in the target region was $E \sim 100-120$ J. The focal plane of each of the guidance systems was located somewhat farther than the target surface, so that the diameter of the light beam in the target plane was $d \approx 400 \mu$. The radiation flux density on the target surface, averaged over the pulse duration, reached $q \lesssim 10^{13}$ W/cm² and, in view of the small convergence angle of the laser beam ($2\alpha = 12^\circ$) past the last component of the focusing system, was independent of the dynamics of the target-corona motion. The targets were solid microspheres of glass (SiO₂) and tin, as well as hollow shells of SiO₂, aluminum oxide Al₂O₃, and polystyrene (C₈H₈)_n with diameters from 2 to 8 μ . The target was suspended on a filament of rubber cement,^[13] the thickness of which could reach 0.5 μ , and was hung from a halter in the form of a slingshot (see Fig. 7 below). A residual pressure inside the hollow microsphere did not exceed 300 Torr. In this series, the focusing of the radiation on the target remained unchanged regardless of the target diameter.

B. Diagnostic apparatus

The energy of the incident radiation and of the radiation reflected from the plasma into the solid angles of the focusing systems was measured with the aid of a multichannel calorimetric setup with digital printouts. In three out of the nine beams, calorimeters were placed behind the target and made it possible to determine the

fraction of the light energy passing through the target. The solid angle in which the transmitted energy was measured was approximately six times larger than the solid angle of the radiation converging on the target. The waveforms of the radiation pulses incident, reflected, and passing through the target were determined with coaxial photocells and also with a photorecorder operating in the slit scanning regime (not indicated in Fig. 1) with a time resolution better than 10^{-10} sec.

The spectral composition of the radiation reflected and scattered by the plasma in the optical band was investigated in different directions with the aid of spectrographs. To investigate the plasma luminosity in the x-ray region of the spectrum ($\lambda \approx 2-10 \text{ \AA}$) we used multi-channel pinpoint cameras which were placed at different angles to the investigated plasma. The spatial resolution reached in these experiments was $\sim 20-25 \mu$ at an image magnification from 1.1 to 2. The pinpoint photographs were registered with high-sensitivity x-ray films of type UF-VR. The spectral distribution of the x-ray photons passing through beryllium and aluminum filters of various thicknesses was investigated with the aid of film detectors^[14] in the soft-photon region ($h\nu < 10$ keV), and with the aid of scintillators and photomultipliers in the region $h\nu > 10$ keV.

To investigate the dynamics of plasma expansion during the first 20 nsec after the start of the heating, we used a system of high-speed multiframe interferometers. Several pulsed light sources separated in space and in time were formed in accordance with the usual optical-delay scheme^[11] with flat mirrors. The light beams formed by the optical delay were directed, making small angles with one another, to a Jamin interferometer tuned to the zeroth order of interference. The interference frames corresponding to different instants of time were photographed with a special multiframe camera in which the images were spatially separated by a prism divider placed in the focal plane of the lens.

To investigate the dynamics of the motion of the shock waves propagating in the gas surrounding the target (the residual gas was hydrogen, deuterium, or air at pressures from 10^{-2} to 10 Torr) we used a multiframe Schlieren photography system in which the formation and spatial separation of the frames were based on a principle similar to that used in the interferometry system. It should be noted that the multiframe Schlieren-photography system has a much better spatial resolution than the shadow method used by us earlier (see, e. g.,^[15]), wherein the inhomogeneity was probed by a parallel beam of light, and the image of the inhomogeneity was produced on a screen placed at a certain distance from the investigated objects by the refraction that redistributed the intensity in the probing beam. It is obvious that in this case the error in the determination of the position of the shock-wave front was proportional to the beam deflection angle in the inhomogeneity and to the distance from the object to the screen. The deflection angle in the inhomogeneity can be estimated from the formula^[16]

$$\epsilon \approx 4.46 \cdot 10^{-14} \lambda^2 \langle dN_e/dr \rangle L,$$

where $\lambda = 5.3 \cdot 10^{-5}$ cm is the wavelength, $L = 2(2R\Delta R - \Delta R^2)^{1/2}$ is the path length of the probing radiation in the shock-wave front (here R is the radius and ΔR is the width of the front of the shock wave), $\langle dN_e/dr \rangle$ is the gradient of the electron density averaged over the path length L . Assuming $R \sim 3$ mm and $\Delta R \sim 0.2$ mm (typical values for 15–20 nsec interference patterns), and $\langle dN_e/dr \rangle \sim 5 \cdot 10^{19}$ cm $^{-4}$ we obtain $\epsilon \sim 2 \times 10^{-3}$ rad.

We can estimate the deflection angle also from the width of the interference fringe, recognizing that $\epsilon = \lambda(1/e - 1/e_0)$, where e is the width of the interference fringe in the presence of the inhomogeneity and e_0 in the absence of perturbations. This estimate yields a value $\epsilon \sim 2.5 \times 10^{-3}$, which agrees well with the first estimate. This indicates that at a distance ~ 500 mm from the screen the uncertainty in the position of the shock-wave front is ~ 1 mm. This accuracy is insufficient to determine the energy absorbed by the plasma from the dynamics of motion of the shock wave,^[1] since a 10% error in the determination of its radius leads to a 50% error in the estimate of the shock-wave energy ($E_{sw} \sim R^5$).

The system chosen by us had a spatial resolution ~ 10 lines/mm. In contrast to^[17], the visualizing diaphragms were chosen to be in the form of holes in a screen placed near the focal plane of the Schlieren objective (ahead of the beam-splitting prism). In such a registration system, the probing radiation deflected in the inhomogeneity was blocked by the diaphragm, while regions with large values of the refractive-index gradient corresponded on the film to the unilluminated zones. To provide the illumination for the optical delays of both high-speed optical diagnostics systems, part of the laser radiation was diverted, after passing through the double-pass amplifiers, to a nonlinear KDP crystal (14), which doubled the frequency of the laser radiation. Thus, the Schlieren and interferometry pictures were recorded at a wavelength $\lambda = 0.532 \mu$; the exposure time of each form was $\tau \leq 10^{-9}$ sec.

To measure the thickness and the homogeneity of the wall of the hollow microspheres, we used an interference procedure which made it possible to determine the distortion of the radiation wavefront passing through the shell. Numerical calculations carried out in^[18] have shown that near the axis of the penetrating beam, up to half the radius of the shell, the shell can be regarded as a spherical lens with focal length that depends on the thickness and diameter of the shell. The displacement interferometer used by us^[19] made it possible to measure the focal distance, and consequently to determine the thickness of the shell accurate to $\sim 0.1 \mu$. The sensitivity of the method to wavefront distortions introduced by the inhomogeneity of the thickness of the hollow microsphere or by its nonsphericity has made it possible to select, in the concluding stage, targets satisfying the experimental requirements.

3. EXPERIMENTAL RESULTS

To obtain maximum temperatures and compressions of the material it is important to determine the influence of the inhomogeneity of the thickness and of the non-uniformity of the illumination of the hollow microsphere on

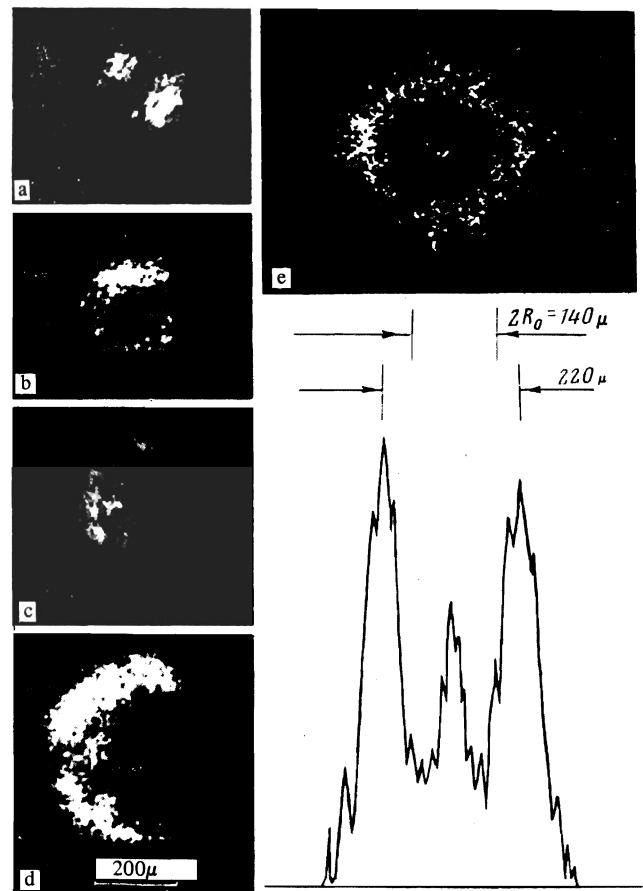


FIG. 3. X-ray pinpoint photographs of plasmas of various targets.

the dynamics of the expansion and on the stability of the compression of the target material. We therefore used pinpoint cameras to determine the luminosity of the plasma of hollow microspheres with different degrees of wall non-uniformity. Figure 3a shows a pinpoint picture for a hollow-shell glass target with radius $R_0 = 70 \mu$, the wall of which was strongly inhomogeneous, with a thickness that varied in the range $\Delta R_0 \sim 3-7 \mu$. Figure 3b shows the pinpoint picture for a flash with a hollow microsphere of the same radius, but with a more uniform wall. In contrast to Fig. 3a, we see the appearance of an external glowing region which assumes, however, a spiral configuration. The average wall thickness was in this case $\Delta R_0 \approx 4 \mu$, and the maximum deviation from this value was of the order of 0.5μ . Finally, Fig. 3c shows a pinpoint picture and a density pattern of its diametral cross section for a flash with a glass target having $R_0 = 70 \mu$ and $\Delta R_0 = 4 \mu$, with wall fluctuations less than 0.3μ . In this case the external glowing region of the plasma acquires a well pronounced spherical shape, and in the center there appears a second glowing region with dimension on the order of the spatial resolution. It is obvious that the causes of these two regions are quite different. The external glowing ring should be attributed to radiation of the corona of the expanding plasma, it being natural to assume that the largest luminosity corresponds to the region near the critical density, where the electron temperature T_e is maximal. Since the pinpoint pattern produces a time-integrated

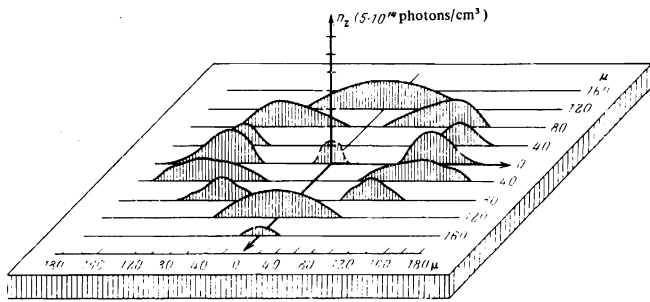


FIG. 4. Map of volume luminosity of plasma corresponding to the pinpoint pattern of Fig. 3e.

record, the appearance of the observed glowing ring corresponds to the plasma region where the luminosity is maximal, or else to the region where the velocity of the motion is minimal. The result differs from those of the experiments^[3,4] in which the diameter of the glowing corona was approximately equal to the initial diameter of the hollow-shell target (the results of^[3,4] are interpreted in^[20]).

It should be noted, however, that the results discussed in the present paper were obtained at lower flux densities than in^[3,4]. The increase in the diameter of the outer luminosity region can be apparently attributed to the fact that at the initial instant of time the region of plasma with critical density moves away from the target surface, in analogy with the case of "sharp" focusing of radiation on a flat target.^[12,21] Another possible explanation is the increased absorption of the radiation in the region of the plasma having one-quarter the critical density, due to the development of parametric instability of the type of decay into two plasmons.^[22] This can lead to a shift of the maximum of the plasma luminosity region towards lower densities.

The appearance of a central glowing region is connected with the fact that the remaining unevaporated part of the hollow-shell target, being decelerated at the center, is compressed and is heated to a high temperature determined by the kinetic energy of the matter moving towards the center. The numerical calculations of the heating and compression of laser-irradiated glass microspheres are given in^[11]. For the flash shown in Fig. 3e it turns out that in the final stage of compression the target constitutes a core with a periphery that is compressed by dozens of times and is relatively cold, and a less dense but much hotter center ($T_e \sim 600$ eV). We note that at a compressed-core lifetime $\tau \sim 10^{-11}$ sec the value of the parameter $n\tau$ is $\sim 5 \times 10^{13}$. The volume compression of the residual gas inside the target amounts in this case to ~ 200 , which is only slightly less than the maximum calculated value.^[11] The result points to instability of the compression of a hollow microsphere with a uniform wall. Experiments with shells of uneven thickness (Figs. 3a and 3b) indicate the absence of compression of the material. In the former case (Fig. 3a), when the initial perturbation amounts to $\sim \pm 60\%$, the growth of the perturbation causes apparently the motion to become turbulent and the recorded integral picture of the radiation becomes smeared out. As a result of inhomogeneities on the order of 10–15% of the

initial thickness, an external glowing region appears, but the central glowing region vanishes, thus indicating the absence of a noticeable compression. Figure 3b shows the limiting case, when the shell has apparently burst. In the case of hollow-shell targets of Al_2O_3 with sufficiently high degree of wall-homogeneity, no compression was observed (Fig. 3c). The apparent reason is the characteristic microstructure of the aluminum oxide.

Figure 4 shows the result of the reduction of a typical pinpoint picture analogous to Fig. 3e, showing the dependence of the volume luminosity of the plasma on the coordinate (the plasma was assumed to be optically thin). By volume luminosity we mean here the number of quanta emitted from a unit volume during the time of registration and passing through the filters that covered the pinpoint camera (in this case the thickness of the beryllium filter was 300μ). The conversion from the photographic-film density $S_z(x)$ to the volume luminosity of the plasma $n_z(r)$ was carried out by using the Abel transformation in accordance with the formula

$$n_z(r) = -\frac{16b^2}{\pi\delta^2} \int_r^{R_z} \frac{[10^{S_z(x)/\gamma}]'}{[x^2-r^2]^{3/2}} dx,$$

which takes into account the geometrical arrangement and the parameters of the pinpoint camera. Here R_z is equal to the value of x at which $S_z(x) = 0.1$; b is the distance from the pinpoint camera to the film, δ is the diameter of the hole in the pinpoint camera, j is the inertia of the film, γ is the contrast factor of the film, determined in each flash. We note that when determining the volume luminosity of the central regions of the plasma, the plasma dimension was assumed to be equal to the spatial resolution of the pinpoint camera. This circumstance, as well as the fact that no account was taken of the absorption of the radiation from the center in the compressed and weakly heated shell, results in the fact that Fig. 4 shows only plots of the minimum luminosity of the central region of the plasma, while the real value of $n_z(0)$ is apparently much larger.

To study the influence of the initial perturbations on the dynamics and on the stability of the compression of spherical microspheres, it is important to determine the experimental criteria for the degree of homogeneity of the radiation $\Delta q/q$ incident of the target. One of the methods of determining $\Delta q/q$ may be variation of the luminosity of different sections of the plasma by inhomogeneous illumination of the target. Figure 3d shows a pinpoint picture of a solid tin target with initial diameter 250μ , illuminated with some of the beams blocked in such a way that the flux density q on one side of the target was larger than on the other side by approximately 2.5 times ($q_1 \approx 8 \times 10^{12}$ W/cm²). Assuming for the dependence of the temperature T_e on the flux density the approximate relation $T_e \sim q^{4/9}$,^[23] we can suppose that the temperatures on the opposite sides of the target differ by approximately 50%, while the plasma luminosity differs by a factor of 2. A similar change in the luminosity was obtained also for glass targets. All this indicates that under the conditions of this ex-

periment the volume luminosity of the plasma depends strongly on the flux density. At large flux densities and for a fully ionized plasma, the dependence can become weaker, since the x-ray intensity ceases to depend on the degree of ionization of the plasma (for recombination radiation, the intensity is proportional to Z^4) and the temperature becomes equalized as a result of the fast growth of the thermal-conductivity coefficient ($k_e \sim T_e^{5/2}$ for classical thermal conductivity).

The electron temperature of the plasma was determined from the ratio of the number of the x-ray photons passing through beryllium filters of various thicknesses.^[24] The measurements have shown that for solid glass microspheres of diameter 100–200 μ these relations agree well with the relations for an equilibrium plasma with temperature $T_e \sim 250$ and 350 eV. For hollow microspheres of the same diameter, the electron temperature usually was $T_e \sim 300$ eV for filters 300 and 500 μ thick, and $T_e \sim 600$ and 700 eV for thickness 300 and 700 μ . This result does not indicate, generally speaking, that the plasma electron velocity distribution function deviates from Maxwellian. The point is that the photograph registers the sum of the x rays from plasma regions with different temperatures, and the temperature furthermore varies with time. This should cause the distribution function measured in this manner to differ from Maxwellian, even though at each instant of time the plasma electrons may be in a state of local thermodynamic equilibrium. The x-ray energy passing through a beryllium filter 300 μ , referred to a solid angle of 4π , ranged (for example for the experiments registered in Figs. 3b and 3e) from 10^{-6} to 10^{-5} J. To determine the total x-ray energy it is necessary to know the exact value of the temperature T_e of the plasma, owing to the strong dependence of the filter transmission coefficient on the form of the x-ray spectral distribution function. Estimates show that not more than 10^{-3} – 10^{-2} J is re-radiated by the plasma in the x-ray band, and this value does apparently play no noticeable role in the energy balance.

The fraction of the optical energy absorbed by the microsphere was determined from the dynamics of the motion of the shock wave^[1] propagating in the residual gas surrounding the target (hydrogen or deuterium). Fig-

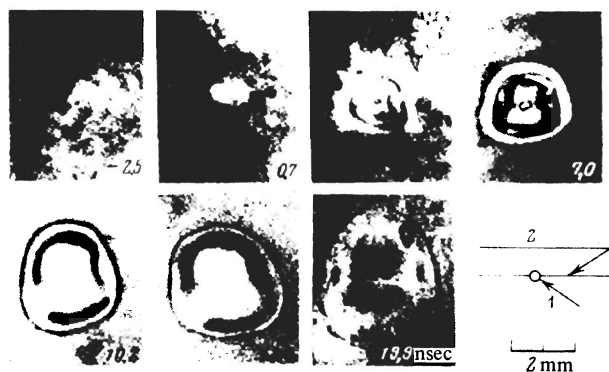


FIG. 5. Interference patterns of laser plasma, corresponding to different instants of time: 1—target, 2—filament.

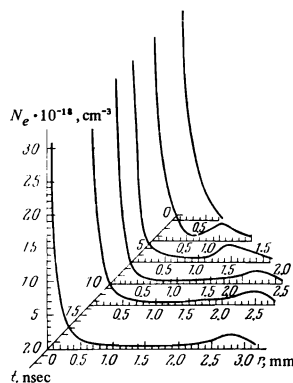


FIG. 6. Spatial distribution of electron density during the initial stage of expansion, obtained by reduction of the interference patterns.

ure 5 shows a seven-frame interference pattern of the shock wave in deuterium ($p = 10$ Torr) obtained in zeroth order of interference and covering the first 20 nsec of the expansion. The target was in this case a glass shell with low degree of homogeneity of the wall with dimensions analogous to the experiment recorded in Fig. 3a.

Figure 6 shows the results of the reduction of an analogous interference pattern; it is seen that several nanoseconds after the start of the heating a shock wave begins to form and is accelerated approximately up to 10–15 nsec. Its subsequent motion is close to that of a shock wave in a homogeneous atmosphere, $R \sim t^\beta$,^[25] but the experimental value of β turned out to be somewhat smaller than 0.4.

Approximately up to 300 nsec, the dynamics of the shock wave, as already noted above, was investigated with the aid of the procedure of multiframe Schlieren photography. Figure 7 shows a characteristic eight-frame Schlieren photograph of a shock wave for a polystyrene hollow microsphere of $\sim 300 \mu$ diameter. The results of the interferometric and Schlieren photographs

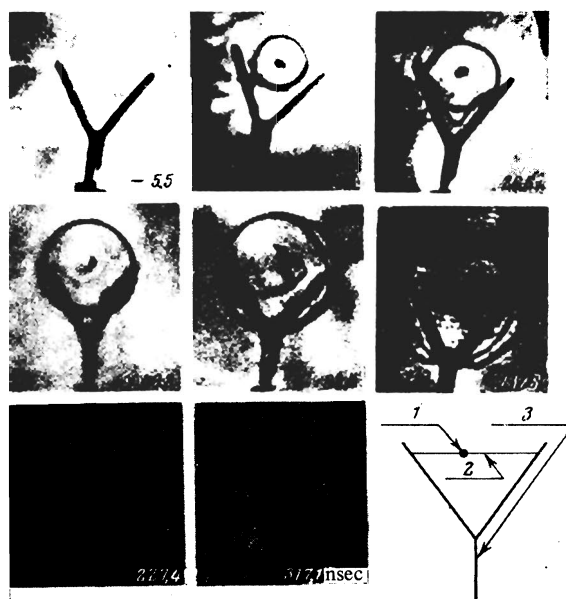


FIG. 7. Characteristic eight-frame Schlieren photograph of shock wave in the residual gas. Target (1)—polystyrene of 300- μ diameter, $\Delta R_0 = 5 \mu$, $E_{sw} \sim 30$ J; 2—filament, 3—suspension of the filament.

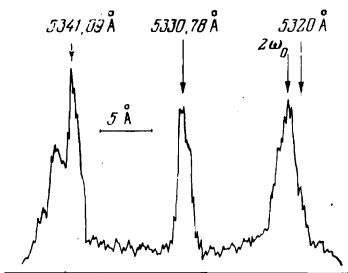


FIG. 8. Spectrum of the second-harmonic line of the heating radiation in the light reflected from the plasma. The references were the neon lines Ne-5341.09 Å and Ne-5330.78 Å.

allow us to conclude that the fraction of the absorbed energy, determined from the shock wave, ranges from 6 to 30–40% of the laser energy, depending on the dimension and the type of the microsphere. Calorimetric measurements of the radiation passing through the target and performed in three beams yielded, however, for the “absorbed” energy values somewhat larger than that determined from the energy of the shock wave, sometimes by a factor 2–3. Thus, for example, for the flash shown in Fig. 3e, the value of the absorbed energy, determined from the shock wave, was approximately 6 J, whereas the calorimetric measurements yielded a value ~15 J.

This difference can apparently be attributed to two causes. The first is connected with the fact that it is possible that not the entire optical energy absorbed by the microsphere is transformed into shock-wave energy. Without dwelling here in detail on the possible causes of this phenomenon, we note only the result of experiments^[15] in which it was shown that the velocity of the shock wave, and consequently its energy, decrease with increasing atomic number of the target material at one and the same absorbed energy.

The other reason is that if the incidence of the light beam on the spherical surface is not exactly normal, the beam can become strongly refracted in the regions of the plasma corona with $N_e < N_{cr}$. Since $n r \sin \theta = \text{const}$ (where n is the refractive index and θ is the angle of incidence of the radiation on the plasma layer), the angle through which the beam is deflected may be arbitrarily large, because n changes from unity in vacuum to zero in the region with the critical density. As a result, the heating radiation does not reach the vicinity of the critical density where the absorption coefficient is maximal. Estimates and calculations of the losses due to refraction (see, e.g.,^[26, 27]) indicate that they can reach dozens of percent of the incident optical energy, and depend strongly on the method whereby the spherical target is illuminated and on the shape of the density profile of the plasma corona. At the present time the role of the parametric effects^[28] that ensure absorption of the laser radiation at large flux densities in the case of flat targets^[22] is not clear, inasmuch as refraction will prevent some of the rays from reaching the densities N_{cr} and $N_{cr}/4$, at which the absorption instabilities develop.

Returning to the results of the present experiment, we can assume that the large value of the “absorbed”

energy obtained with the aid of the calorimetric procedure is connected with the fact that some of the rays are refracted and do not strike the calorimeters located behind the target. It appears therefore that we must assume that the calorimetric method yields the maximum value of the absorbed energy, while the optical methods yield the minimum value. The energy reflected by the plasma at the frequency of the heating radiation was measured in the solid angles of the focusing systems of three beams with the aid of coaxial photocells and calorimeters. The reflection coefficient, i.e., the ratio of the optical energy reflected from the plasma into the aperture of the lens and the energy of the given beam, differed in the different observation channels by not more than 30–40%, and amounted, for example for a glass shell of 140 μ diameter, to $R_L \leq 0.05\%$, with a weak dependence on the shell thickness. Assuming that the scattering is isotropic in the solid angle 4π sr, we obtain the total reflection coefficient $R_{4\pi} \sim 2\%$. It must be stated, however, that when spherical targets are heated by radiation of multichannel lasers, it is impossible to determine the fractions of the scattered and refracted radiation of neighboring beams in the reflected radiation.

Figure 8 shows a spectrogram of the lines of the second harmonic frequency of the heating radiation, obtained by observation in the solid angle of one of the focusing systems for an SiO_2 shell. In^[29] there was proposed a method of determining the temperature T_e in the critical-density region, from the displacement of the $2\omega_0$ line relative to the nominal value 5320 Å, under the assumption that the appearance of this line is due to the development of decay instability. For the flux densities in the described experiment, the formula connecting the shift of the maximum of the line with the electron temperature becomes ($\Delta\lambda$ in Å, T_e in keV)

$$\Delta\lambda = (20ZT_e/A)^{1/4}.$$

For $\Delta\lambda \approx 1.5$ Å, $A_{av} = 20$, and $Z = 8$ we obtain $T_e \approx 280$ eV, in good agreement with the data obtained with x rays. At a flux density $q \sim 10^{14}$ W/cm² at a narrow heating-radiation line, the structure of the $2\omega_0$ line becomes much more complicated, and an asymmetrical pedestal, shifted towards the red end of the spectrum, is observed.

In conclusion, the authors thank Yu. S. Leonov, F. I. Matveeva, Yu. A. Merkul'ev, L. M. Ochkaeva, and E. R. Rychkova for help in preparing and selecting the targets, and also A. A. Erokhin, B. D. Makarov, and No. V. Novikov for help with the experiments.

¹N. G. Basov, O. N. Krokhin, G. V. Sklizkov, S. I. Fedotov, and A. S. Shikanov, Zh. Eksp. Teor. Fiz. 62, 203 (1972) [Sov. Phys. JETP 35, 109 (1972)].

²N. G. Basov, E. G. Gamaly, O. N. Krokhin, Yu. A. Mikhailov, G. V. Sklizkov, and S. I. Fedotov, Laser Interaction and Related Plasma Phenomena 3, Plenum Press, New York, 1974; N. G. Basov, O. N. Korkhin, G. V. Sklizkov, and S. I. Fedotov, Tr. Fiz. Inst. Akad. Nauk SSSR 76, 146 (1974).

³P. M. Campbell, G. Charatis, and G. R. Montry, Phys. Rev. Lett. 34, 74 (1975).

- ⁴B. R. Guscott, G. Charatis, J. S. Hildum, R. R. Johnson, F. J. Mayer, N. K. Moncur, P. E. Solomon, and C. E. Thomas, Preprint KMSF-U346, Seventh European Conf. on Controlled Fusion, Lausanne, Switzerland, Sept. 1-5, 1975.
- ⁵G. H. McCall and R. L. Morse, *Laser Focus* 10, 40 (1974).
- ⁶J. H. Nuckolls, J. L. Emmett, H. G. Ahlstrom, C. D. Hedricks, L. W. Coleman, J. A. Blaze, J. H. Holzrichter, and D. G. Dahlbacka, Preprint UCRL-76957, Seventh European Conf. on Controlled Fusion, Lausanne, Switzerland, Sept. 1-5, 1975.
- ⁷N. G. Basov, A. A. Kologrivov, O. H. Krokhin, A. A. Rupasov, G. V. Sklizkov, and A. S. Shikanov, *Pis'ma Zh. Eksp. Teor. Fiz.* 23, 474 (1976) [*JETP Lett.* 23, 428 (1976)].
- ⁸Yu. V. Afanas'ev, N. G. Basov, P. P. Volosevich, E. G. Gamalii, O. N. Krokhin, S. P. Kurdyumov, E. I. Levanov, V. B. Rozanov, A. A. Samarskii, and A. N. Tikhonov, *Pis'ma Zh. Eksp. Teor. Fiz.* 21, 150 (1975) [*JETP Lett.* 21, 68 (1975)].
- ⁹J. Nuckolls, J. Lindl, W. Mead, A. Thiessen, L. Wood, and G. Zimmerman, Fifth IAEA Conf. on Plasma Physics and Controlled Nucl. Fusion Research, Tokyo, Japan, Nov. 11-15, 1974, paper IAEA-CN-33/F 5-4.
- ¹⁰G. S. Fraley, W. P. Gula, D. B. Henderson, R. L. McCrory, R. C. Malone, R. J. Mason, and R. L. Morse, Fifth IAEA Conf. on Plasma Physics and Controlled Nucl. Fusion Research, Tokyo, Japan, Nov. 11-15, 1974, paper IAEA-CN-33/F 5-5.
- ¹¹Yu. V. Afanas'ev, P. P. Volosevich, E. G. Gamalii, O. N. Krokhin, S. P. Kurdyumov, E. I. Levanov, and V. B. Rozanov, *Pis'ma Zh. Eksp. Teor. Fiz.* 23, 470 (1976) [*JETP Lett.* 23, 425 (1976)].
- ¹²Yu. A. Zakharenkov, N. N. Zorev, O. N. Korkhin, Yu. A. Mikhaïlov, A. A. Rupasov, G. V. Sklizkov, and A. S. Shikanov, *Zh. Eksp. Teor. Fiz.* 70, 547 (1976) [*Sov. Phys. JETP* 43, 382 (1976)].
- ¹³E. G. Gamalii, A. I. Isakov, Yu. A. Merkul'ev, A. I. Nikitenko, E. R. Rychkova, and G. V. Sklizkov, *Kvantovaya Elektron (Moscow)* 2, 1043 (1974); E. R. Rychkova, *ibid.*, 1048 [*Sov. J. Quantum Electron.* 5, 568 (1975)].
- ¹⁴O. N. Krokhin, Yu. A. Mikhaïlov, A. A. Rupasov, V. P. Silin, G. V. Sklizkov, and A. S. Shikanov, *Pis'ma Zh. Eksp. Teor. Fiz.* 20, 239 (1974) [*JETP Lett.* 20, 105 (1974)].
- ¹⁵O. N. Krokhin, G. V. Sklizkov, and A. S. Shikanov, *Tr. Fiz. Inst. Akad. Nauk SSSR* 85, 143 (1975).
- ¹⁶R. W. Ladenburg *et al.*, *Physical Measurements in Gas Dynamics and Combustion*, Princeton, 1954.
- ¹⁷A. S. Shikanov and Yu. A. Zakharenkov, Proc. of the Eleventh Congress on High Speed Photography, Sept. 1974.
- ¹⁸R. R. Stone, D. W. Gregg, and P. C. Souers, *J. Appl. Phys.* 46, 2693 (1975).
- ¹⁹P. Hariharan and D. Sen, *J. Opt. Soc. Am.* 49, 1105 (1959).
- ²⁰K. A. Brueckner, P. M. Campbell, and R. A. Grandey, *Nucl. Fusion* 15, 471 (1975).
- ²¹G. N. Korkhin, Yu. A. Mikhaïlov, A. A. Rupasov, G. V. Sklizkov, A. S. Shikanov, Yu. A. Zakharenkov, and N. N. Zorev, Proc. Twelfth Intern. Conf. on Phenomena in Ionized Gases, Eindhoven, Netherlands, August 18-22, 1975.
- ²²N. G. Basov, O. N. Krokhin, V. V. Pustavalov, A. A. Rupasov, V. P. Silin, G. V. Sklizkov, V. T. Tikhonchuk, and A. S. Shikanov, *Zh. Eksp. Teor. Fiz.* 67, 118 (1974) [*Sov. Phys. JETP* 40, 61 (1975)].
- ²³O. N. Krokhin, in *Physics of High Energy Density*, N. Y. - London, Acad. Press, 1971, p. 278.
- ²⁴F. C. Jahoda, E. M. Little, W. E. Quinn, G. A. Sawyer, and T. F. Stratton, *Phys. Rev.* 119, 843 (1960).
- ²⁵V. P. Korobeinikov, N. S. Mel'nikova, and E. V. Ryazanov, *Teoriya tochechnogo vzryva (Theory of Point-Source Explosion)*, Fizmatgiz, 1961.
- ²⁶K. Brueckner, R. Cover, J. Howard, F. J. Mayer, and D. Mitrovich, Preprint KMSF-U176.
- ²⁷M. Lubin, E. Goldman, J. Soures, L. Goldman, W. Friedman, S. Letzring, J. Albritton, P. Koch, and B. Yaakovi, Fifth IAEA Conf. on Plasma Physics and Controlled Nucl. Fusion Research, Tokyo, Japan, Nov. 11-15, 1974, paper IAEA-CN-33/F 4-2.
- ²⁸V. P. Silin, *Parametricheskoe vozdeistvie izlucheniya bol'shoi moschnosti na plazmu (Parametric Action of High-Power Radiation on Plasma)*, Nauka, 1973.
- ²⁹O. N. Krokhin, V. V. Pustovalov, A. A. Rupasov, V. P. Silin, G. V. Sklizkov, A. N. Starodub, V. T. Tikhonchuk, and A. S. Shikanov, *Pis'ma Zh. Eksp. Teor. Fiz.* 22, 47 (1975) [*JETP Lett.* 22, 21 (1975)].

Translated by J. G. Adashko